

See discussions, stats, and author profiles for this publication at: <https://www.researchgate.net/publication/283558933>

Beyond Frangi: An improved multiscale vesselness filter

Article in *Proceedings of SPIE - The International Society for Optical Engineering* · March 2015

DOI: 10.1117/12.2081147

CITATIONS

102

READS

10,245

4 authors, including:



[Ziga Spiclin](#)

University of Ljubljana

94 PUBLICATIONS 1,411 CITATIONS

SEE PROFILE

Beyond Frangi: an improved multiscale vesselness filter

Tim Jerman*, Franjo Pernuš, Boštjan Likar, and Žiga Špiclin

University of Ljubljana, Faculty of Electrical Engineering
Tržaška 25, SI-1000 Ljubljana, Slovenia

ABSTRACT

Vascular diseases are among the top three causes of death in the developed countries. Effective diagnosis of vascular pathologies from angiographic images is therefore very important and usually relies on segmentation and visualization of vascular structures. To enhance the vascular structures prior to their segmentation and visualization, and to suppress non-vascular structures and image noise, the filters enhancing vascular structures are used extensively. Even though several enhancement filters are widely used, the responses of these filters are typically not uniform between vessels of different radii and, compared to the response in the central part of vessels, their response is lower at vessels' edges and bifurcations, and vascular pathologies like aneurysm. In this paper, we propose a novel enhancement filter based on ratio of multiscale Hessian eigenvalues, which yields a close-to-uniform response in all vascular structures and accurately enhances the border between the vascular structures and the background. The proposed and four state-of-the-art enhancement filters were evaluated and compared on a 3D synthetic image containing tubular structures and a clinical dataset of 15 cerebral 3D digitally subtracted angiograms with manual expert segmentations. The evaluation was based on quantitative metrics of segmentation performance, computed as area under the precision-recall curve, signal-to-noise ratio of the vessel enhancement and the response uniformity within vascular structures. The proposed filter achieved the best scores in all three metrics and thus has a high potential to further improve the performance of existing or encourage the development of more advanced methods for segmentation and visualization of vascular structures.

Keywords: Angiography, vessels, bifurcations, aneurysms, nodules, multiscale enhancement filter, Hessian eigenvalues, quantitative evaluation.

1. INTRODUCTION

Vascular diseases are one of the leading cause of disability and death in the developed countries.^{1,2} From 1990 to 2010 the number of people affected by vascular diseases increased due to the increase in population and ageing,² whereas the majority of the diseases led to premature death. Therefore, an early and effective diagnosis and treatment is essential in order to reduce the devastating impact of these diseases.

Imaging of vascular structures is an important paraclinical tool for the diagnosis of cardiovascular and circulatory diseases. Three angiographic imaging modalities are widely used: computed tomography angiography (CTA), magnetic resonance angiography (MRA), and digital subtraction angiography (DSA).³ Because of high image resolution and high diagnostic accuracy, DSA became the reference standard, especially in imaging cerebral vasculature, for the detection of various vascular pathologies like vessel stenosis, aneurysm,^{4,5} arteriovenous malformation to name a few. Nevertheless, DSA is an invasive and costly imaging technique. CTA and MRA are non-invasive and less costly alternatives, but generally deliver images with lower resolution compared to DSA.⁶

Inspection of three-dimensional (3D) angiographic images can be a tedious and time consuming task. To help the clinician quickly inspect the angiographic images and identify the vascular pathologies, computer algorithms have been developed for the enhancement, extraction and visualization of vascular structures based on angiographic images.^{7,8} Most extensively used image preprocessing techniques are multiscale vessel enhancement filters,^{9–11} which are usually applied prior to segmentation and visualization. Hence, the performance of vessel segmentation and visualization algorithms may critically depend on the performance of enhancement filters.

Most state-of-the-art enhancement filters^{9–11} employ the analysis of 2nd order derivatives of image intensity, which is encoded in a Hessian matrix. The core of each filter is the enhancement function, a mathematical

*E-mail: tim.jerman@fe.uni-lj.si, Telephone: +386 1 4768 873, Web: www.lit.fe.uni-lj.si

expression involving the eigenvalues of the Hessian matrix, based on which the response of the filter is computed. Quantitative evaluation revealed important drawbacks of these enhancement functions like (i) poor response uniformity on vascular structures inherent to the design of enhancement functions, e.g. the dependence of response on the contrast of vascular structures and on vessel radius, and (ii) suppression of vessels and other vascular structures with elliptic cross-sections, e.g. vessel stenosis or spindle-shaped aneurysms, and (iii) suppression of nearly spherical structures, namely bifurcations and vascular pathologies like aneurysms and nodules. The observed characteristics may inhibit a proper segmentation and/or visualization of the vascular structures.

In this paper, we propose a novel enhancement function, which cancels the dependence on the contrast of structures it aims to enhance by employing the ratio of Hessian eigenvalues. On synthetic and real 3D angiographic images, the proposed function yields a close-to-uniform response on vascular structures, including vessels of different radii as well as structures with non-circular cross-section like bifurcations and aneurysms. An objective evaluation and comparison to the existing enhancement filters revealed an improved performance of the proposed filter, which, therefore, has a high potential to improve the performance of those state-of-the-art segmentation and visualization methods relying on prior enhancement of the vascular structures.⁷

2. RELATED WORK

Enhancement filters are scalar functions $\mathcal{V} : \mathbb{R} \rightarrow \mathbb{R}$, which selectively amplify a specific local intensity profile or structure in an image. Several enhancement filters^{9–13} characterize the local structure by analyzing 2nd order intensity derivatives or Hessian at each point in the image. To enhance the local structures of various sizes, the analysis is typically performed on a Gaussian scale space of the image.

Let $I(\mathbf{x})$ denote the intensity of a D -dimensional image at coordinate $\mathbf{x} = [x_1, \dots, x_D]^T$, then the Hessian of $I(\mathbf{x})$ at scale s is represented by a $D \times D$ matrix defined as:

$$H_{ij}(\mathbf{x}, s) = s^2 I(\mathbf{x}) * \frac{\partial^2}{\partial x_i \partial x_j} G(\mathbf{x}, s) \text{ for } i, j = 1, \dots, D, \quad (1)$$

where $G(\mathbf{x}, s) = (2\pi s^2)^{-D/2} \exp(-\mathbf{x}^T \mathbf{x} / 2s^2)$ is a D -variate Gaussian and $*$ denotes convolution.

Differentiation and thus a selective enhancement of the local image structures, based on their shape and foreground vs. background brightness, can be determined irrespective of their orientation by analyzing the signs and magnitudes of Hessian eigenvalues. The eigenvalues are obtained through eigenvalue decomposition of the Hessian matrix, i.e. $\text{eig } \mathcal{H}(\mathbf{x}, s) \rightarrow \lambda_i, i = 1, \dots, D$, which can be computed fast for 2×2 and 3×3 Hessian matrices with an analytical method developed by Kopp.¹⁴ Table 1 lists the local image structures that can be identified by the analysis of Hessian eigenvalues.






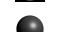
Ideally, the enhancement filters \mathcal{V} are indicator functions of a selected set of relations of Hessian eigenvalues given in Table 1. Let the eigenvalues λ_i of \mathcal{H} be sorted according to their magnitude: $|\lambda_i| \leq |\lambda_{i+1}|; i = 1, \dots, D - 1$. In 3D images ($D = 3$), for example, vessels resemble tube-like or elongated structures, which can be indicated by the following relations of the Hessian eigenvalues: $\lambda_2 \approx \lambda_3 \wedge |\lambda_{2,3}| \gg 0 \wedge \lambda_1 \approx 0$. Moreover, the positive (negative) sign of λ_2 and λ_3 indicates a dark (bright) vessel on a bright (dark) background. For other structures, or a set of structures, the eigenvalue relations can be derived from Table 1 in a similar manner.

A multiscale filter response $\mathcal{F}(\mathbf{x})$ is obtained by maximizing a given enhancement function \mathcal{V} , at each point \mathbf{x} , over a range of different scales s as:

$$\mathcal{F}(\mathbf{x}) = \sup \left\{ \mathcal{V}[\text{eig } \mathcal{H}(\mathbf{x}, s)] : s_{\min} \leq s \leq s_{\max} \right\} \quad (2)$$

The values of s_{\min} and s_{\max} are selected according to the respective minimal and maximal expected size of the structures of interest.

Table 1. Structure based on Hessian eigenvalues analysis.⁹ Note that eigenvalues are sorted according to magnitude as $|\lambda_i| \leq |\lambda_{i+1}|$; $i = 1, \dots, D-1$, whereas H=high and L=low magnitude and +/- indicates the sign of the eigenvalue.

3D			
Structure	λ_1	λ_2	λ_3
	L	L	H-
	L	L	H+
	L	H-	H-
	L	H+	H+
	H-	H-	H-
	H+	H+	H+

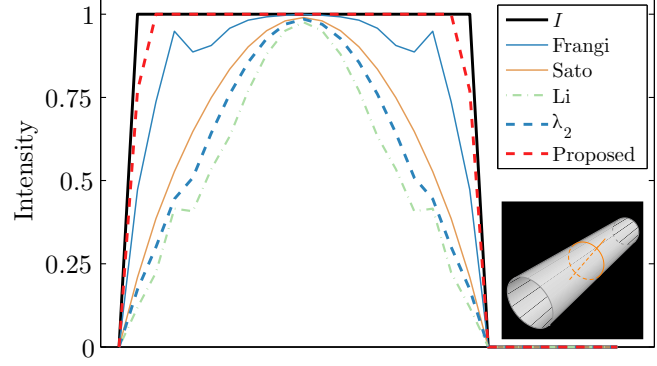


Figure 1. Normalized responses of four and the proposed enhancement functions along a line passing intersecting a synthetic tube with intensity profile I . The response of proposed function accurately follows the raw intensity profile as opposed to other functions.

2.1 Enhancement of Vascular Structures

Vascular structures generally consist of elongated structures. However, bifurcations and some structural vascular pathologies like aneurysms and nodules may resemble spherical structures. To enhance both elongated and spherical structures in 3D the enhancement function \mathcal{V} needs to indicate the following Hessian eigenvalue relations: $\lambda_2 \approx \lambda_3 \wedge |\lambda_{2,3}| \gg 0$, while the value of λ_1 can be arbitrary.

Here we review several state-of-the-art filters aimed at the enhancement of vascular structures. Any filter that differentiated between elongated and spherical structures was modified so as to account for the both structural shapes. The reason is that the enhancement filters may otherwise suppress the vascular structures such as bifurcations and vascular pathologies like aneurysms. Because angiographic images such as 3D-DSA or CTA normally depict the vascular structures as bright objects on dark background, we define all enhancement functions \mathcal{V} to yield non-zero response only when $\lambda_3 \leq \lambda_2 < 0$. If vascular structures appear dark with respect to background, the inequalities in the aforementioned conditions need to be inverted.

The most widely used is Frangi's filter⁹ aimed at the enhancement of vessels (elongated structures). For our purpose, the factor introduced for the suppression of spherical structures was removed, thus the enhancement function becomes

$$\mathcal{V}_F = \left(1 - \exp\left(-\frac{\mathcal{R}_A^2}{2\alpha^2}\right)\right) \left(1 - \exp\left(-\frac{\mathcal{S}^2}{2\kappa^2}\right)\right), \quad (3)$$

where $\mathcal{S} = \sqrt{\lambda_1^2 + \lambda_2^2 + \lambda_3^2}$ is the 2nd order measure of image structureness, while $\mathcal{R}_A = \lambda_2/\lambda_3$ distinguishes between tubular and planar structures. Parameters α and κ control the sensitivity of measures \mathcal{R}_A and \mathcal{S} .⁹

The original Sato's enhancement function¹⁰ also involves a factor to suppress spherical structures, which we removed to arrive at:

$$\mathcal{V}_S = \lambda_3 \left(\frac{\lambda_2}{\lambda_3}\right)^\gamma. \quad (4)$$

Parameter γ controls the sensitivity to elongated structures and is typically set either to 0.5 or 1, which simplifies the expression (4) into $\sqrt{\lambda_3\lambda_2}$ and λ_2 , respectively. We will refer to the former as Sato's enhancement function and to the latter as λ_2 .

Li *et al.*¹¹ proposed a similar enhancement function, which, without the suppression of spherical structures, is expressed as:

$$\mathcal{V}_L = \frac{\lambda_2^2}{|\lambda_3|}, \quad (5)$$

which can be factored into $|\lambda_2| \times \lambda_2/\lambda_3$. According to Li *et al.* the first factor represents the magnitude and the second the likelihood of an elongated or spherical structure, since $\lambda_2/\lambda_3 \rightarrow 0$ only for plane-like structures.

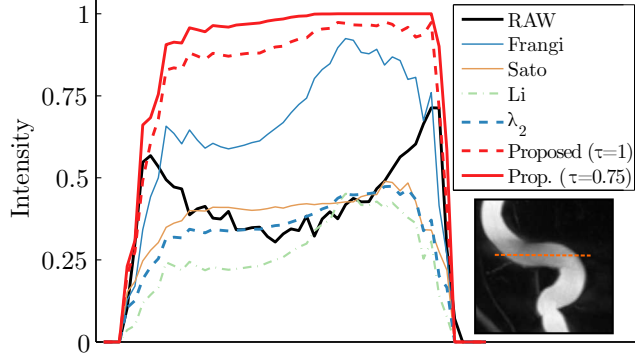


Figure 2. Normalized intensity profile of raw 3D-DSA image and corresponding normalized responses of several enhancement functions along a line passing the centerline of an internal carotid artery. The raw image intensities vary along the line, which has an adverse affect on some of the enhancement functions.

The expressions of all the aforementioned enhancement functions are, in some way, proportional to the magnitude or squared magnitude of λ_2 or λ_3 . By using $e^x \approx 1 + x$ to approximate the second factor in (3) we get

$$\left(1 - \exp\left(-\frac{\mathcal{S}^2}{2\kappa^2}\right)\right) \approx \frac{1}{2\kappa^2} (\lambda_2^2 + \lambda_3^2), \quad (6)$$

which shows that the Frangi's function (3) is proportional to the squared magnitude of λ_2 and λ_3 . The dependence of enhancement functions on the magnitude of λ_2 or λ_3 is imposed mainly so suppress noise in image regions with low and uniform intensities, where all eigenvalues have low and similar magnitudes.

The linear or higher order dependence on magnitudes of λ_2 or λ_3 , however, leads to two important drawbacks. First, for an ideal structure with a uniform bright foreground and uniform dark background, the response of, e.g., λ_2 is not uniform in a cross-section of an elongated or spherical structure. Instead, $|\lambda_2|$ peaks at the center of the structure and then progressively decreases towards the periphery of its circular cross-section. This can be verified in Fig. 1 that shows the responses of several enhancement filters along a line passing along the cross-section of a synthetic image of a tube, which is bright with uniform intensity on a dark and uniform background.

Second, any 1st or higher order scaling of image intensity reflects in the magnitudes of λ_2 and λ_3 and, therefore, also in the response of enhancement filters. Because angiographic imagery is mostly acquired while administering contrast agent into the blood flow, or otherwise relies on blood flow-related enhancement (e.g. TOF-MRA), any variations in the blood flow characteristics (e.g. turbulent flow at obstacles), or variations in the level of contrast agent, may result in high variations of raw image intensity. The phenomena can be observed in a cross-section of internal carotid on cerebral 3D-DSA, which is shown in Fig. 2 together with the impact on the corresponding responses of enhancement filters sampled along the centerline of internal carotid.

Among the reviewed enhancement functions, the Frangi's function has the highest response uniformity on objects with uniform intensity, possibly confirming the reason for its widespread use. Nevertheless, as linear, or higher order, dependence of the enhancement functions on λ_2 or λ_3 was established as a source of poor response uniformity and of high sensitivity to object contrast, the response of Frangi's and other functions can be further improved. Moreover, the enhancement functions aim to indicate the relation $\lambda_2 \approx \lambda_3$, which will effectively suppress vessels with elliptic cross-sections. Namely, the value of ratio λ_2/λ_3 corresponds to the ratio of minor and major semi axes of a vessel's cross-section and will be 1 for spheric or otherwise less than 1 for elliptic vessel cross-sections.

3. PROPOSED ENHANCEMENT FILTER

We hypothesize that by devising an enhancement function in the form of a ratio of eigenvalues, which is not directly proportional to any of the eigenvalues and, at the same time, is robust to low-magnitudes of the eigenvalues, we can achieve a response that is close-to-uniform and invariant to object contrast. These two characteristics are critical for accurate and balanced enhancement of the vascular structures.

Peeters et al.¹⁵ review several enhancement functions used to measure structural isotropy and anisotropy of diffusion tensors, some of which can also be applied to Hessian matrices. One measure based on the ratio of eigenvalues, that is otherwise used for the detection of nearly spherical diffusion tensors,¹⁶ is volume ratio:

$$VR = \lambda_1 \lambda_2 \lambda_3 \left[\frac{3}{\lambda_1 + \lambda_2 + \lambda_3} \right]^3. \quad (7)$$

The response of VR is between 0 and 1. To indicate both spherical and elongated structures the VR can be modified by introducing $\lambda_1 \rightarrow (\lambda_2 - \lambda_1)$, which yields one possible enhancement function:

$$\mathcal{V} = (\lambda_2 - \lambda_1) \lambda_2 \lambda_3 \left[\frac{3}{2\lambda_2 - \lambda_1 + \lambda_3} \right]^3. \quad (8)$$

The enhancement function is based on a ratio of eigenvalues and, since $|\lambda_1| \leq |\lambda_2|$, has a response between 0 and 1. To indicate $\lambda_2 \approx \lambda_3$ the value of λ_1 is generally irrelevant, hence it can be omitted in (8).

The response of such an enhancement function, however, is ill-defined at low magnitudes of λ_2 and λ_3 and may thus be susceptible to noise in image regions with uniform intensity. To ensure robustness of the enhancement function to low-magnitudes of λ_2 and λ_3 , we propose to regularize the value of λ_3 at each scale s as:

$$\lambda_\rho = \begin{cases} \lambda_3 & \text{if } \lambda_3 < \tau \min_{\mathbf{x}} \lambda_3(\mathbf{x}, s), \\ \tau \min_{\mathbf{x}} \lambda_3(\mathbf{x}, s) & \text{otherwise,} \end{cases} \quad (9)$$

where τ is a cutoff threshold between zero and one. Choosing a high value of τ increases the difference between the magnitudes of λ_2 and λ_3 for structures with low contrast, which otherwise have low magnitude of λ_2 and λ_3 . Note that we want to enhance only bright structures on dark background, which must have all the eigenvalues negative, therefore λ_3 with highest magnitude is obtained as $\min_{\mathbf{x}} \lambda_3(\mathbf{x}, s)$. The enhancement function becomes:

$$\mathcal{V} = \lambda_2^2 \lambda_\rho \left[\frac{3}{2\lambda_2 + \lambda_\rho} \right]^3. \quad (10)$$

To account for vascular structures with elliptic cross-sections the enhancement function should, besides $\lambda_2 \approx \lambda_3$, also indicate the relations with $\lambda_2 \geq \lambda_3$ (note that $\lambda_2, \lambda_3 < 0$). We consider sufficient to account for vascular structures with elliptic cross-sections with ratio λ_2/λ_3 from 0.5 to 1, which corresponds to the eigenvalue relation: $\lambda_2 \leq \lambda_3/2$. Because the value of λ_3 is regularized we indicate the relation $\lambda_2 \leq \lambda_\rho/2$, which requires the enhancement function (10) to return a value of 1 when $\lambda_2 \leq \lambda_\rho/2$ or otherwise have a smooth transition between 0 and 1. This can be achieved by fixing the response to 1 for $\lambda_2 \leq \lambda_\rho/2$, while otherwise inserting $\lambda_\rho \rightarrow (\lambda_\rho - \lambda_2)$ into (10) to obtain a smooth transition when $\lambda_\rho/2 \leq \lambda_2 \leq 0$. Finally, the proposed enhancement function is computed as:

$$\mathcal{V}_P = \begin{cases} 0 & \text{if } \lambda_2 > 0 \wedge \lambda_3 > 0, \\ 1 & \text{if } \lambda_2 \leq \lambda_\rho/2, \\ \lambda_2^2 (\lambda_\rho - \lambda_2) \left(\frac{3}{\lambda_2 + \lambda_\rho} \right)^3 & \text{otherwise.} \end{cases} \quad (11)$$

The proposed enhancement function is based on a ratio of eigenvalues with the range response values from 0 to 1. An example response of $\mathcal{V}_P(\tau = 1)$ is shown in Fig. 1 along a line intersecting the synthetic tube. The response closely follows the uniform intensity profile of the tubular structure. Decreasing τ generally increases λ_ρ , since there is a higher likelihood that $\lambda_2 > \lambda_\rho/2$, for which \mathcal{V}_P is set to 1. The consequence of this is, in general, a more uniform response on bright structures for $\tau < 1$. In case of varying contrast of raw image intensities, as observed for the internal carotid artery in Fig. 2, the proposed enhancement function gives a uniform response, owing to the use of eigenvalue ratio in (11). Hence, as hypothesized the proposed enhancement function yields a high and highly uniform response in the presence of varying contrast of the structures of interest.

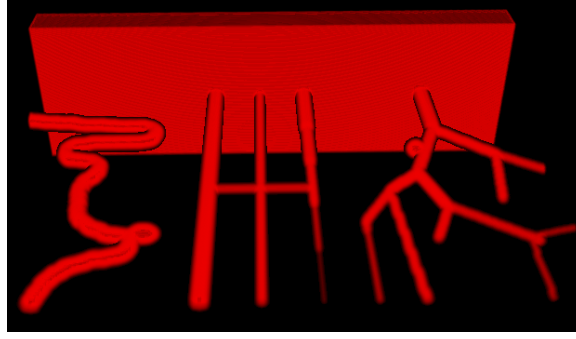


Figure 3. A 3D visualization of the synthetic image, which contains structures commonly found in angiograms: tubular structures with various radii, bends, bifurcations and vascular pathologies such as aneurysms, which are depicted as hyper-ellipses attached to the tubular structures.

4. EXPERIMENTS

The performance of the proposed, Frangi's,⁹ Sato's,¹⁰ Li's,¹¹ and λ_2 ⁸ (a variant of Sato's filter) enhancement filters were evaluated and compared on a synthetic 3D image and a clinical dataset consisting of 15 cerebral 3D digitally subtracted angiograms (DSAs). The responses of the vessel enhancement filters were computed over a range of scales from $s_{min} = 0.5$ to $s_{max} = 2.5$ mm with step size of 0.5 mm. The same range was used for all evaluated filters and all 15 images from the clinical dataset, as for the synthetic image. To compare the responses of the vessel enhancement filters their output values were normalized to range $[0, 1]$.

4.1 Angiographic Datasets

A 3D synthetic image with a grid of $230 \times 320 \times 100$ voxels with isotropic spacing of 0.5 mm was created such that it contained structures similar to those typically found in (cerebral) angiograms: tubular structures with various radii, bends, bifurcations and aneurysms (see Fig. 3). The largest cross-section of the 3D vascular structures was positioned on a common 2D plane so as to enable a direct visual comparison of the filters' responses. Because clinical images are corrupted by noise, a comparable level of Poisson noise was added to the synthetic image.

The clinical dataset consisted of fifteen 3D-DSA images acquired during patient screening with the Siemens Axiom Artis dBA angiography system. The size of the acquired angiograms was $512 \times 512 \times 391$ voxels with isotropic spacing of 0.46 mm. In each image a region of interest ($200 \times 200 \times 200$) that contained the majority of the vascular structures was manually selected. The vascular structures including vessels, bifurcations and vascular pathologies were manually segmented by an expert and the obtained reference segmentations were used to objectively evaluate and compare the filters' responses.

4.2 Evaluation Metrics

All filters were quantitatively evaluated using three performance metrics: 1) area under the precision-recall curve (AUC-PR),¹⁷ 2) signal-to-noise ratio (SNR), and median of the normalized filter's response inside the reference segmentation (MedNR). The values of AUC-PR range between zero and one, where higher values indicate a better segmentation performance compared to the reference segmentation. The uniformity of the response inside the vasculature is measured by the MedNR, which has values between zero and one. A more uniform filter response has values of MedNR closer to one. Improvement of visual contrast due to the use of enhancement filters was quantified by computing the SNR between the filter responses in the regions of the reference segmentations of vascular structures and the responses in the remaining regions. A high value of SNR corresponds to a high and uniform response in regions of the targeted vascular structures and, at the same time, to a low response inside of the remaining regions.

5. RESULTS

The medial cross-sections of the 3D synthetic image and the corresponding enhanced responses of the proposed ($\tau = 1$), λ_2 , Sato's, Frangi's, and Li's enhancement function are presented in Fig. 4. Among all the evaluated

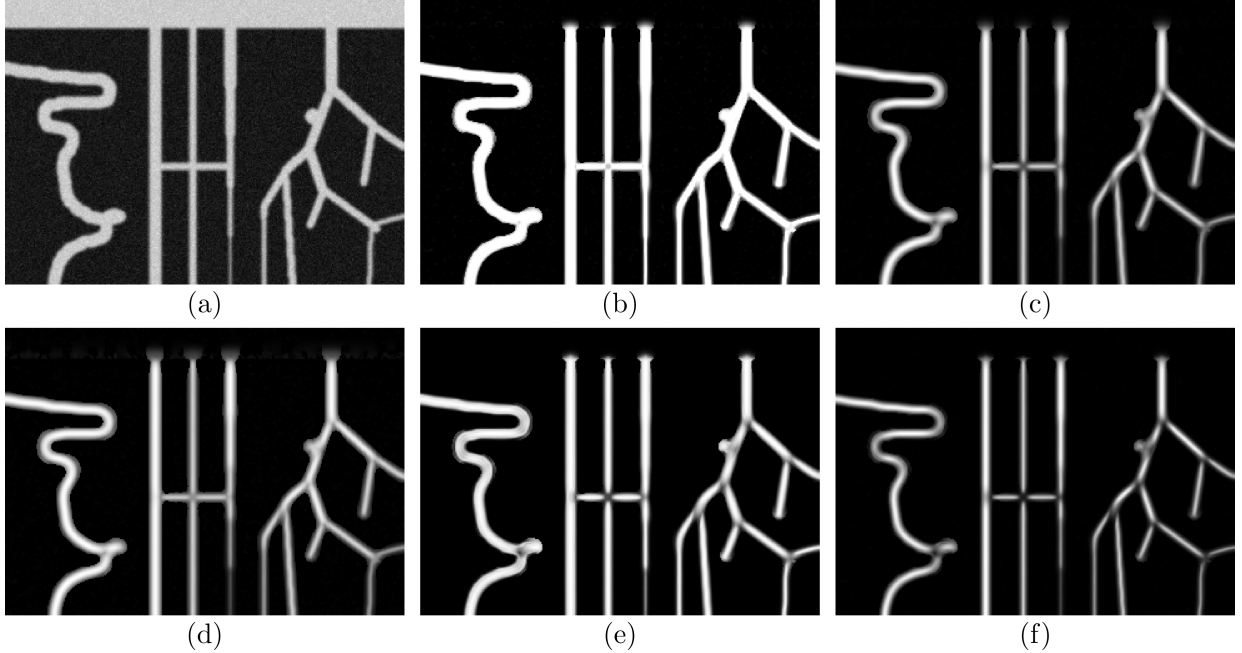


Figure 4. Medial cross-sections of (a) the synthetic 3D image, and the corresponding responses of enhancement filters: (b) the proposed, (c) λ_2 , (d) Sato's, (e) Frangi's, and (f) Li's.

Table 2. Quantitative evaluation metrics of the enhancement filters, computed for their responses on 3D synthetic image (Fig. 4).

Filter	AUC-PR	SNR	MedNR
λ_2	0.96	2.10	0.43
Sato	0.98	2.81	0.53
Frangi	0.95	1.95	0.51
Li	0.93	1.48	0.29
Proposed ($\tau = 1$)	0.97	3.58	0.94

function, the proposed enhancement function gave a very high and most uniform response inside all the vascular structures, irrespective of their size. Moreover, the response was high also on bifurcations, which other function failed to enhance. This was indicated by reduced overall uniformity measured by MedNR (Table 2). Another drawback of the state-of-the-art function is the dependence of response value on the vessel's width with distinctly lower response inside smaller structures compared to the larger ones. For this reason, smaller vessels may not be extracted by a segmentation or missed due to low contrast on volume renderings of the response. On the other hand, the use of the proposed function resulted in the enhancement of all vascular structures, which are clearly visible in the response (Fig. 4).

Evaluation metrics (AUC-PR, SNR, MedNR) computed for the responses of the proposed and four other enhancement filters obtained on the synthetic image are presented in Table 2. The proposed filter had by far the highest SNR and MedNR values and, at the same time, a comparably high value of AUC-PR. Consequently, compared to other enhancement filters, the proposed filter achieved a significantly higher visual contrast enhancement of the vessel structures as seen in Fig. 4.

The proposed enhancement function has only one tuning parameter τ , which was otherwise fixed to one in the experiments. The effect of varying τ on the evaluation metrics was assessed on the synthetic image and is shown in Fig. 5. By lowering τ from one towards zero the uniformity of the filter's response rises (higher MedNR). At the same time, the AUC-PR decreases, however, the difference is insignificant in the range of $\tau = [0.5\ 1]$.

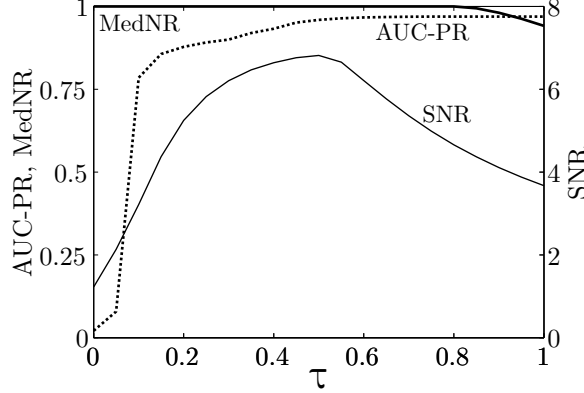


Figure 5. Response of the proposed enhancement function with respect to varying τ in terms of metrics AUC-PR, SNR and MedNR. The metrics were computed for responses on the 3D synthetic image.

Table 3. Means of the evaluation metrics of the responses of enhancement filters computed on 15 cerebral 3D-DSA images.

Filter	AUC-PR	SNR	MedNR
λ_2	0.87	1.53	0.23
Sato	0.89	1.78	0.27
Frangi	0.79	1.76	0.48
Li	0.81	1.19	0.15
Proposed ($\tau = 1$)	0.89	2.05	0.62

Therefore, τ can be easily selected on this range without sacrificing the performance of enhancement function. Lowering τ also increases the SNR value, which peaks around value $\tau = 0.5$.

Evaluation metrics AUC-PR, SNR, MedNR were also computed for the fifteen 3D-DSA images from the clinical dataset. For each enhancement filter the mean values over the 15 response images are summarized in Table 3. The presented values are in accordance with the results obtained on the 3D synthetic image. The proposed filter had the highest values of all three evaluation metrics, thus proving the superior to the other tested filters.

A volume rendering of a 3D-DSA from the clinical dataset and of the response of the proposed enhancement filter is shown in Fig. 6. Compared to the volume rendering of the raw image, the rendering of the response of proposed filter reduces the intensity variations inside of the vascular structures (clearly seen on the internal carotid artery).

Visual comparison of the enhancement of vascular structures on a 3D-DSA by all tested filters, shown as maximum intensity projection (MIP) of the raw intensity image and the MIPs of corresponding filter responses, is provided in Fig. 7. The responses of state-of-the-art filter are clearly lower for small vessels compared the responses in larger vessels, whereas the proposed filter has high response values in all the vascular structures. For this reason, the segmentation or visualization of the smallest vessels immediately improve with the use of proposed filter.

6. DISCUSSION

The enhancement of the vascular structures in the angiographic images may facilitate their visualization and automated extraction, which must be performed accurately, as they play an important role in the detection of vascular pathologies.⁷ Hessian based enhancement filters have been previously demonstrated as an important step in the extraction of vascular structures.⁹ Recently, a faster approach for Hessian eigenvalue computation was demonstrated,¹⁸ which effectively halves the computation times and, thereby, increases the potential for

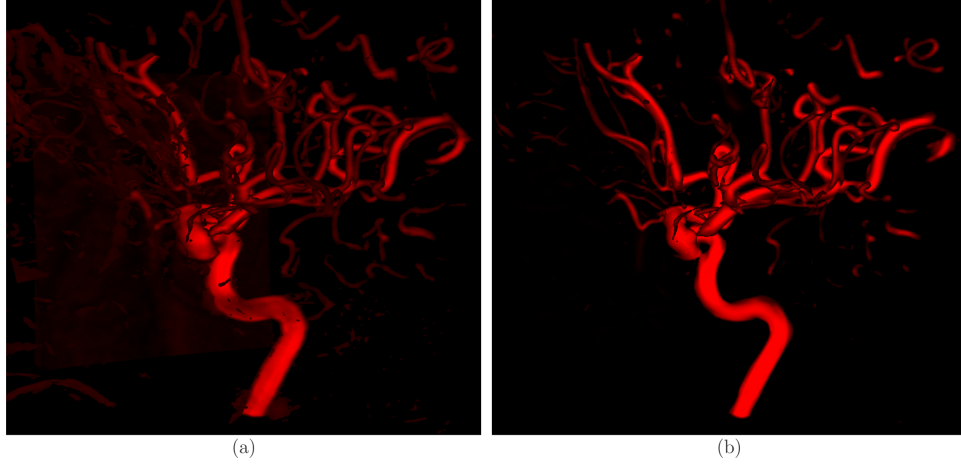


Figure 6. Volume rendering of (a) the raw 3D-DSA image from the clinical dataset and (b) the rendering of corresponding response of the proposed enhancement filter.

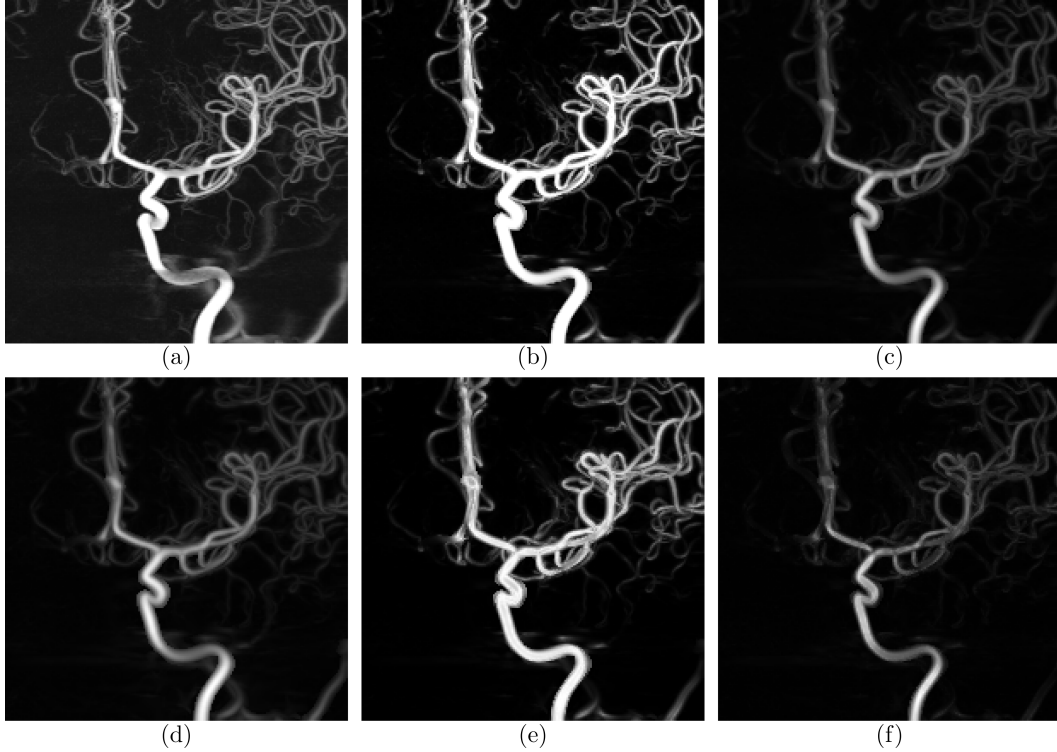


Figure 7. Maximum intensity projections of (a) raw 3D-DSA image from the clinical dataset and of the corresponding responses of enhancement filters: (b) the proposed, (c) λ_2 , (d) Sato's, (e) Frangi's, and (f) Li's.

practical use of the enhancement filters. In this paper, we introduced a novel enhancement filter based on the ratio of multiscale Hessian eigenvalues. The proposed filter was evaluated and compared to four state-of-the-art filters^{8–11} on a 3D synthetic image and on a clinical dataset of 15 cerebral 3D-DSA images. Three quantitative evaluation metrics were used: area under the precision-recall curve (AUC-PR), signal-to-noise ratio (SNR), and median of the normalized response inside of the reference segmentations (MedNR). The AUC-PR, SNR and MedNR measured the respective segmentation performance, visual contrast enhancement and uniformity of the filters' responses.

A quantitative evaluation and comparison of the tested filters showed an improved performance of the pro-

posed filter over the state-of-the-art filters. The proposed filter had by far the highest values of SNR and MedNR for both the synthetic image and the images in clinical dataset. This can be observed as a high and highly uniform response in the vascular structures independently of the vessel size (Fig. 4). The increase of the response uniformity did not hinder the segmentation performance of the filter as the evaluation showed comparably high values of AUC-PR compared to the best state-of-the-art filter. If needed, the uniformity of the response can be further increased by lowering the proposed filter's only parameter τ towards 0.5 (Fig. 5). A lower value of τ increases the SNR and MedNR, while the AUC-PR lowers insignificantly.

The major drawbacks of the state-of-the-art filters are (i) poor response uniformity on vascular structures and (ii) suppression of vessels and other vascular structures with non-circular cross-sections. Poor response uniformity can be observed in Figs. 4 and 7 as a low response at bifurcations and smaller vessels, while a high response is present at other vessels. Moreover, all the vessels can not be clearly visible when a filter response is visualized. These characteristics can reduce the performance of vessel segmentation algorithms that rely on the Hessian based enhancement filters. Since the proposed filter has a highly uniform response, and also enhances vascular structures non-circular cross-sections, it has a high potential to improve the performance of those state-of-the-art segmentation and visualization methods (e.g. Fig. 6) relying on prior enhancement of the vascular structures.⁷

ACKNOWLEDGEMENTS

This research was supported by the Ministry of Education, Science and Sport, Slovenia, under grants J2-5473, L2-5472, and L2-4072.

REFERENCES

- [1] Lopez, A. D., Mathers, C. D., Ezzati, M., Jamison, D. T., and Murray, C. J., eds., [*Global Burden of Disease and Risk Factors*], World Bank, Washington (DC) (2006).
- [2] Murray, C. J. L., Vos, T., Lozano, R., Naghavi, et al., "Disability-adjusted life years (DALYs) for 291 diseases and injuries in 21 regions, 1990–2010: a systematic analysis for the global burden of disease study 2010," *The Lancet* **380**, 2197–2223 (Dec. 2012).
- [3] Sailer, A. M. H., Grutters, J. P., Wildberger, J. E., Hofman, P. A., Wilmink, J. T., and van Zwam, W. H., "Cost-effectiveness of CTA, MRA and DSA in patients with non-traumatic subarachnoid haemorrhage," *Insights Imaging* **4**, 499–507 (July 2013).
- [4] Villablanca, J. P., Jahan, R., Hooshi, P., Lim, S., Duckwiler, G., Patel, A., Sayre, J., Martin, N., Frazee, J., Bentson, J., and Viñuela, F., "Detection and characterization of very small cerebral aneurysms by using 2d and 3d helical CT angiography," *Am J Neuroradiol* **23**, 1187–1198 (Aug. 2002).
- [5] van Rooij, W., Sprengers, M., de Gast, A., Peluso, J., and Sluzewski, M., "3d rotational angiography: The new gold standard in the detection of additional intracranial aneurysms," *Am. J. Neuroradiol.* **29**, 976–979 (Feb. 2008).
- [6] White, P. M., Wardlaw, J. M., and Easton, V., "Can noninvasive imaging accurately depict intracranial aneurysms? a systematic review," *Radiology* **217**(2), 361–370 (2000).
- [7] Lesage, D., Angelini, E. D., Bloch, I., and Funka-Lea, G., "A review of 3d vessel lumen segmentation techniques: Models, features and extraction schemes," *Med. Image Anal.* **13** (Dec. 2009).
- [8] Wiemker, R., Klinder, T., Bergtholdt, M., Meetz, K., Carlsen, I. C., and Buelow, T., "A radial structure tensor and its use for shape-encoding medical visualization of tubular and nodular structures," *IEEE Trans. Vis. Comput. Graph.* **19**, 353–366 (Mar. 2013).
- [9] Frangi, A. F., Niessen, W. J., Vincken, K. L., and Viergever, M. A., "Multiscale vessel enhancement filtering," in [*Medical Image Computing and Computer-Assisted Intervention - Miccai'98*], Wells, W. M., Colchester, A., and Delp, S., eds., **1496**, 130–137, Springer-Verlag Berlin, Berlin (1998).
- [10] Sato, Y., Westin, C. F., Bhalerao, A., Nakajima, S., Shiraga, N., Tamura, S., and Kikinis, R., "Tissue classification based on 3d local intensity structures for volume rendering," *IEEE T. Vis. Comput. Gr.* **6**, 160–180 (June 2000).

- [11] Li, Q., Sone, S., and Doi, K., “Selective enhancement filters for nodules, vessels, and airway walls in two- and three-dimensional CT scans,” *Med. phys.* **30**, 2040–2051 (Aug. 2003).
- [12] Koller, T., Gerig, G., Szekely, G., and Dettwiler, D., “Multiscale detection of curvilinear structures in 2-d and 3-d image data,” in [, *Fifth International Conference on Computer Vision, 1995. Proceedings*], 864–869 (June 1995).
- [13] Lorenz, C., Carlsen, I.-C., Buzug, T. M., Fassnacht, C., and Weese, J., “A multi-scale line filter with automatic scale selection based on the hessian matrix for medical image segmentation,” in [*Scale-Space Theory in Computer Vision*], Romeny, B. t. H., Florack, L., Koenderink, J., and Viergever, M., eds., *Lecture Notes in Computer Science*, 152–163, Springer Berlin Heidelberg (Jan. 1997).
- [14] Kopp, J., “Efficient numerical diagonalization of hermitian 3x3 matrices,” *International Journal of Modern Physics C* **19**, 523–548 (Mar. 2008). arXiv:physics/0610206.
- [15] Peeters, T. H. J. M., Rodrigues, P. R., Vilanova, A., and Romeny, B. M. t. H., “Analysis of distance/similarity measures for diffusion tensor imaging,” in [*Visualization and Processing of Tensor Fields*], Laidlaw, D. and Weickert, J., eds., *Mathematics and Visualization*, 113–136, Springer Berlin Heidelberg (Jan. 2009).
- [16] Pierpaoli, C. and Basser, P. J., “Toward a quantitative assessment of diffusion anisotropy,” *Magn. Reson. Med.* **36**, 893–906 (Dec. 1996).
- [17] Fawcett, T., “An introduction to ROC analysis,” *Pattern Recogn. Lett.* **27**, 861–874 (June 2006).
- [18] Yang, S.-F. and Cheng, C.-H., “Fast computation of hessian-based enhancement filters for medical images,” *Comput. Meth. Prog. Bio.* **116**, 215–225 (Oct. 2014).